

Oxygen vacancies and V co-doped Co_3O_4 prepared by ion implantation boosts oxygen evolution catalysis

Bo Sun(孙博), Dong He(贺栋), Hongbo Wang(王宏博), Jiangchao Liu(刘江超), Zunjian Ke(柯尊健), Li Cheng(程莉), and Xiangheng Xiao(肖湘衡)

Citation: Chin. Phys. B, 2021, 30 (**10**): 106102. DOI: 10.1088/1674-1056/ac1339
Journal homepage: http://cpb.iphy.ac.cn; http://iopscience.iop.org/cpb

What follows is a list of articles you may be interested in

Formation of nano-twinned 3C-SiC grains in Fe-implanted 6H-SiC after 1500-℃ annealing

Zheng Han(韩铮), Xu Wang(王旭), Jiao Wang(王娇), Qing Liao(廖庆), and Bingsheng Li(李炳生)
Chin. Phys. B, 2021, 30 (**8**): 086107. DOI: 10.1088/1674-1056/abff43

Mechanism of defect evolution in H^+ and He^+ implanted InP

Ren-Jie Liu(刘仁杰), Jia-Jie Lin(林家杰), N Daghbouj, Jia-Liang Sun(孙嘉良), Tian-Gui You(游天桂), Peng Gao(高鹏), Nie-Feng Sun(孙聂枫), and Min Liao(廖敏)
Chin. Phys. B, 2021, 30 (**8**): 086104. DOI: 10.1088/1674-1056/abf640

Optical spectroscopy study of damage evolution in 6H-SiC by H$_{2}^{ + }$ implantation

Yong Wang(王勇), Qing Liao(廖庆), Ming Liu(刘茗), Peng-Fei Zheng(郑鹏飞), Xinyu Gao(高新宇), Zheng Jia(贾政), Shuai Xu(徐帅), and Bing-Sheng Li(李炳生)
Chin. Phys. B, 2021, 30 (**5**): 056106. DOI: 10.1088/1674-1056/abe9a7

Evolution of ion-irradiated point defect concentration by cluster dynamics simulation

Shuaishuai Feng(冯帅帅), Shasha Lv(吕沙沙), Liang Chen(陈良), and Zhengcao Li(李正操)
Chin. Phys. B, 2021, 30 (**5**): 056105. DOI: 10.1088/1674-1056/abf102

Structure and luminescence of *a*-plane GaN on *r*-plane sapphire substrate modified by Si implantation

Lijie Huang(黄黎杰), Lin Li(李琳), Zhen Shang(尚震), Mao Wang(王茂), Junjie Kang(康俊杰), Wei Luo(罗巍), Zhiwen Liang(梁智文), Slawomir Prucnal, Ulrich Kentsch, Yanda Ji(吉彦达), Fabi Zhang(张法碧), Qi Wang(王琦), Ye Yuan(袁冶), Qian Sun(孙钱), Shengqiang Zhou(周生强), and Xinqiang Wang(王新强)
Chin. Phys. B, 2021, 30 (**5**): 056104. DOI: 10.1088/1674-1056/abd76a

---

SPECIAL TOPIC — Ion beam modification of materials and applications

Oxygen vacancies and V co-doped Co_3O_4 prepared by ion implantation boosts oxygen evolution catalysis*

Bo Sun(孙博), Dong He(贺栋), Hongbo Wang(王宏博), Jiangchao Liu(刘江超), Zunjian Ke(柯尊健), Li Cheng(程莉)†, and Xiangheng Xiao(肖湘衡)‡

Department of Physics, Hubei Nuclear Solid Physics Key Laboratory, Wuhan University, Wuhan 430072, China

(Received 27 May 2021; revised manuscript received 4 July 2021; accepted manuscript online 12 July 2021)

Introducing heteroatoms and defects is a significant strategy to improve oxygen evolution reaction (OER) performance of electrocatalysts. However, the synergistic interaction of the heteroatom and defect still needs further investigations. Herein, we demonstrated an oxygen vacancy-rich vanadium-doped Co_3O_4 (V–O_v–Co_3O_4), fabricated by V-ion implantation, could be used for high-efficient OER catalysis. X-ray photoelectron spectra (XPS) and density functional theory (DFT) calculations show that the charge density of Co atom increased, and the reaction barrier of reaction pathway from O^* to HOO^* decreased. V–O_v–Co_3O_4 catalyst shows a low overpotential of 329 mV to maintain current density of 10 mA·cm^{-2}, and a small Tafel slope of 74.5 mV·dec^{-1}. This modification provides us with valuable perception for future design of heteroatom-doped and defect-based electrocatalysts.

Keywords: ion implantation, oxygen vacancy, oxygen evolution reaction, heteroatom doping

PACS: 61.80.−x, 61.72.U−, 88.30.em, 63.20.dk **DOI:** 10.1088/1674-1056/ac1339

1. Introduction

In the face of the rapid growth of energy demand and the consumption of traditional fossil fuels, it is urgent need to develop sustainable energy sources.[1,2] As is well known, hydrogen has long been considered as an ideal energy carrier to replace traditional fossil fuels because of its high energy density and carbon neutral.[3,4] As one of the most promising methods for hydrogen production, electrochemical water-splitting mainly includes hydrogen evolution reaction (HER) and oxygen evolution reaction (OER). However, as a sluggish kinetics process, OER involves a four-electron and four protons transfer process, which impedes the energy conversion efficiency of hydrogen production by water electrolysis.[1,5–8] Currently, the commercial catalysts for water splitting are noble metals and their compounds such as ruthenium dioxide (RuO_2)/iridium dioxide (IrO_2) for OER in practical application, but their high price and instability limit the large-scale commercial application of those electrocatalysts.[9–11] Thus, it is urgent to develop earth-abundant and high-efficient catalysts to replace noble metal-based catalysts for OER catalysis.

Recently, transition metal oxides (TMO) such as Ni/Co/Fe-based oxides have been widely concerned by researchers, considered to be the promising OER catalysts. Among TMO materials, Co_3O_4, B-doped Co_3O_4, CoO/Co_3O_4, $CoFe_2O_4$, *etc.*, as potential non-precious metal OER electrocatalysts have been intensively investigated.[12–15] Specifically, Co_3O_4 have been widely regarded as the well-studied OER catalysts due to low cost, multivalence oxidation states, and high stabilities.[16,17] However, the relatively poor conductivity and unfavorable absorption ability to oxygen-containing reaction intermediates of Co-based TMOs impede their practical application.[18] Therefore, improving the conductivity and properly adjust the absorption behavior of Co_3O_4 during the OER process is expected for a long time.[19,20] Recently, defects and oxygen vacancies (O_v) have been intensively explored as effective method to coordinate the electronic structure of Co_3O_4 toward improving catalytic activity.[18,21] Creating oxygen vacancies are effective strategy to enhances the adsorption of intermediates and promote the electronic conductivity of Co_3O_4, and oxygen vacancies filled with OH• first could facilitate the pre-oxidation has been confirmed by operando spectroscopy and electrochemical measurement for Co_3O_4 with oxygen vacancies (O_v–Co_3O_4).[12,22] Furthermore, doping suitable heteroatoms is widely used to improve conductivity and further enhance its OER performance of Co_3O_4. Although it has been reported that doping heteroatoms into cobalt oxide can improve the OER activity, but more work has focused on cation doping with some atomic whose size similar to Co atoms, limited by conventional chemical doping methods.[23] So far, compared with iron, nickel and manganese, there are rarely studies on

*Project supported by the National Natural Science Foundation of China (Grant Nos. 12025503, U1867215, and U1932134), Hubei Provincial Natural Science Foundation (Grant No. 2019CFA036), the Fundamental Research Funds for the Central Universities, China (Grant No. 2042020kf0211), and China Postdoctoral Science Foundation (Grant No. 2020M682429).

†Corresponding author. E-mail: lcheng@whu.edu.cn

‡Corresponding author. E-mail: xxh@whu.edu.cn

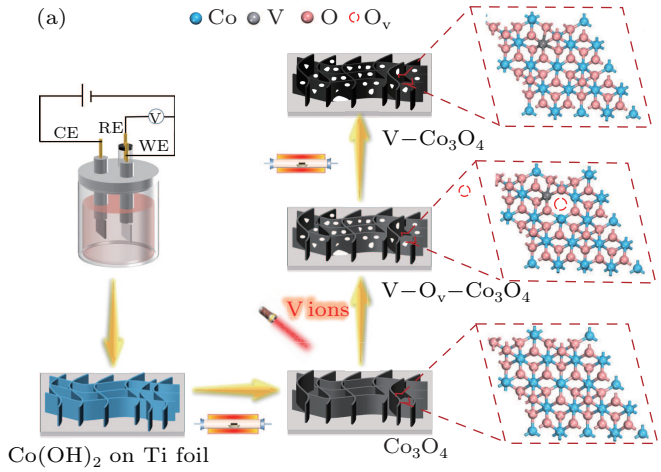
© 2021 Chinese Physical Society and IOP Publishing Ltd

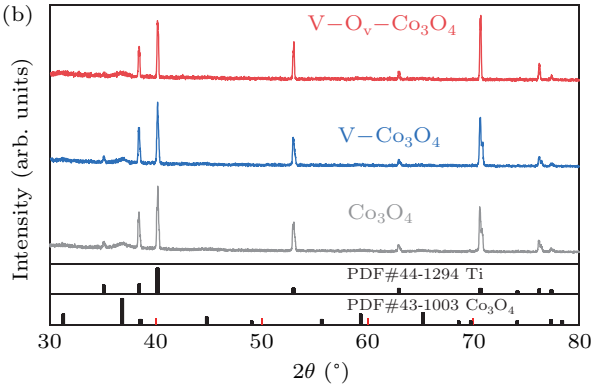
vanadium as a dopant for electrocatalysts, so it is very meaningful to develop cobalt oxides with V-doping and oxygen vacancies.[24–26] Meanwhile, it is very important and meaningful to analyze on the synergistic interaction of V dopant and oxygen vacancies. However, limited by methods that simultaneously generate oxygen vacancies and V doping, the mechanism of the synergistic interaction still needs to be studied in depth. The development and application of simple, efficient and controllable doping and defect generated methods have always been the focus and deficiencies of research.

Herein, we report an oxygen vacancy and V co-doped Co_3O_4 (V–O_v–Co_3O_4) as an OER catalyst, prepared by novel and controllable V ion implantation. The increased of low valence state of Co species (demonstrated by XPS results) in V–Ov–Co_3O_4 is higher than that of pristine Co_3O_4 (Co_3O_4) and V–Co_3O_4 represent the generated of oxygen vacancies by V ions implantation. At the contributed of the vanadium doping and the generation oxygen vacancies for the optimization of electronic properties, the overpotential of V–O_v–Co_3O_4 on Ti foil was reduced to 329 mV, compared with Co_3O_4 (403 mV) and V–Co_3O_4 (381 mV). The Tafel slope of V–Ov–Co_3O_4 is much smaller, 74.5 mV·dec^{-1}, which is obviously better than that of Co_3O_4 (172 mV·dec^{-1}) and V–Co_3O_4 (152.9 mV·dec^{-1}). The density functional theory (DFT) simulations confirm synergistic interaction between V doping and oxygen vacancies generated by ions implantation. Apart from improving conductivity, another factor for the significantly improved OER activity is due to the energy barrier from O* to HOO* was decreased, caused by the increase of the charge density around Co atoms and the improvement of HOO* absorption.

2. Results and discussion

Cobalt hydroxide is prepared on Ti foil substrate using a general electrochemical deposition method, and it was converted to Co_3O_4 after a thermal annealing process.[27] And then, Co_3O_4 was subjected to vanadium ion-implantation at 40 kV (V–O_v–Co_3O_4) to the dosage of 4×10^{16} ions·cm^{-2}, and V– Co_3O_4 was prepared from annealed V–O_v–Co_3O_4 (Fig. 1(a)) in air atmosphere. The x-ray diffraction (XRD) patterns of Co_3O_4, V–Co_3O_4, and V–O_v–Co_3O_4 were firstly tested as show in Fig. 1(b). The diffraction peaks of Co_3O_4 sample located at 31.2°, 36.7°, 59.2°, and 65.2° , can be corresponded to (200), (211), (321), and (400) planes of the spinel Co_3O_4 phase (JCPDS No. 43-1003), apart from diffraction peaks belongs to Ti foil. Meanwhile, the V–O_v–Co_3O_4 (irradiated Co_3O_4) and V–Co_3O_4 (annealed V–O_v–Co_3O_4) exhibited the similar diffraction pattern as Co_3O_4, indicating no obvious phase changes occurred during the implantation process. The morphology change of the high-energy vanadium-ion implantation Co_3O_4 was analyzed by scanning electron microscope (SEM). Figure 1(c) showed that the Co_3O_4 sample was consisted of smooth and continuous two-dimensional (2D) nanosheets oriented and interconnected other. After the high-energy vanadium-ion implantation, broken surface and porous framework was observed for V–O_v–Co_3O_4 (Fig. 1(d)) which was constructed by ion sputtering, and the similar morphology was also found in the sample of V–Co_3O_4 (Fig. S1). Energy dispersive spectrometer (EDS) reveals that Co, O, and V elements homogenously distribution throughout the V–O_v–Co_3O_4 (Fig. 1(e)). Compared to Co_3O_4 (Fig. S2), the elemental mapping images of V–O_v–Co_3O_4 and V–Co_3O_4 (Fig. S1) suggested that V element was successfully homogenously doped into Co_3O_4 after the V-ion implantation. The vanadium content in V–O_v–Co_3O_4 is 0.34 wt%. In short, V-ion implantation realized the doping of V element and increases the surface area in Co_3O_4 nanosheets, which was supported by SEM and XRD results.





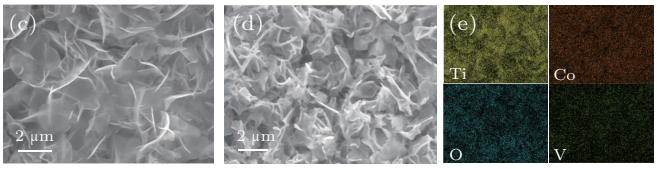


Fig. 1. Illustration of fabrication, structural, and morphology characterization. (a) Schematic diagram of preparation Co_3O_4, V–Co_3O_4, and V–O_v–Co_3O_4. (b) XRD patterns of Co_3O_4, V–Co_3O_4, and V–O_v–Co_3O_4. SEM images of (c) Co_3O_4. SEM images (d) and elemental mapping images (e) of V–O_v–Co_3O_4.

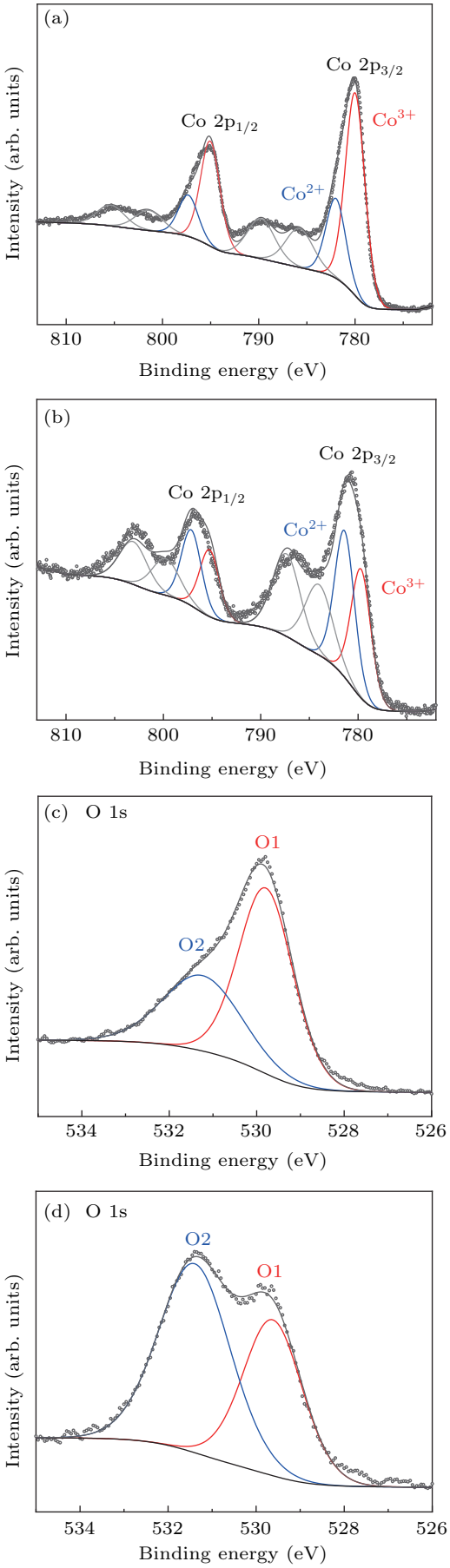


Fig. 2. Electronic structure characterization: Co 2p XPS spectra of Co_3O_4 (a) and V–O_v–Co_3O_4 (b). The O 1s XPS for Co_3O_4 (c) and V–O_v–Co_3O_4 (d).

Since electrochemical reaction usually occurs on the solid–liquid interface between the surface of the electrocatalyst and the electrolyte, probing the surface electronic structure of the prepared catalyst samples is crucial to study the OER reaction. Hence, x-ray photoelectron spectroscopy (XPS), as a universal and super-sensitive instrument, was used to study electronic states on prepared catalyst surfaces. Figures 2(a), 2(b), and S3 show that the Co 2p XPS spectra of Co_3O_4, V–Co_3O_4, V–O_v–Co_3O_4. Two typical peaks at around 795 eV and 779.9 eV should be specified to Co $2p_{1/2}$ and Co $2p_{3/2}$ for Co_3O_4 and V–Co_3O_4, respectively. After V-ion implantation, it could be distinctly observed that the peaks of the two new satellites are located at 787 eV and 803 eV, respectively, and the Co 2p of V–O_v–Co_3O_4 peaks shift negatively (about 0.2 eV) (Fig. 2(b)), which indicates the increase of electron density in the Co species. In order to explore the differences in the chemical valence of Co atoms before and after V-ion implantation, Co 2p spectra were fitted. There are two fitted peaks, located at 779.8 eV and 781 eV, which belong to Co^{3+} oxidation state and Co^{2+} oxidation state for Co $2p_{3/2}$, respectively.[27,28] From the fitted result, it is obviously exhibited that atomic ratios of Co^{2+}/Co^{3+} of V–O_v–Co_3O_4 (1.1) is significantly higher than that Co^{2+}/Co^{3+} of Co_3O_4 (0.4). The higher atomic ratios indicate that there is a higher proportion of Co^{2+} in the V-ion-implanted Co_3O_4, and oxygen vacancies were created by sputtering effect of V-ion implantation. The atomic ratios of Co^{2+}/Co^{3+} of V–Co_3O_4 are similar to that of Co_3O_4. The oxygen vacancies in V–Co_3O_4 were also validated by fine-scanned O1s spectrum. Figures 2(c), 2(d), and S4 shows that there are two typically oxygen peaks located at 529.8 eV (O1) and 531.6 eV (O2) of Co_3O_4, V–Co_3O_4 and V–O_v–Co_3O_4.[27,29] O1 is identified as a typical metal–oxygen bonds. The O2 with higher binding energy peak is considered to be oxygen defect species.[27] Comparing with O2 peak of Co_3O_4 and V–Co_3O_4, the stronger intensity O2 peak of V–O_v–Co_3O_4 (Fig. 2(d)) reveals a large number of oxygen defect sites with Co^{2+} species are formed. The results shown in XPS for three samples indicated that Co^{2+} species were produced with creating oxygen vacancies by V-ion implantation. Combined with the characterization of structure, morphology, and composition, it is confirmed that V-ion implantation can realize both of the doping of V element and the generation of oxygen vacancy in Co_3O_4 without distinct phase change.

The role of oxygen defect and doped V sites on Co_3O_4 nanosheets were investigated herein by carefully evaluating the as-prepared catalysts performance for OER activity. All electrocatalytic performance tests are performed in a three-electrode cell with workstation (CHI 760E) at 25 °C in 1-M KOH solution. Due to Co_3O_4, V–Co_3O_4, and V–O_v–Co_3O_4 electrocatalysts were supported on Ti foil, which were tested directly as work electrodes. The OER electrocatalytic activity

of the prepared samples were measured by polarization curves with a scan rate of 5 mV·s^{-1} and the data were presented with IR corrected by 90%. Figure 3(a) illustrates OER polarization curves of the Co_3O_4, V–Co_3O_4, and V–O_v–Co_3O_4. The V–O_v–Co_3O_4 catalysts displayed outstanding OER catalytic activity. To maintain a current density of 10 mA·cm^{-2}, the V–O_v–Co_3O_4 only needs overpotential of 329 mV. The V–Co_3O_4 (381 mV) and Co_3O_4 (403 mV) need higher overpotential, indicating the great OER catalytic performance of V-ion implantation Co_3O_4. Tafel slope is a commonly used descriptor for studying the catalytic mechanism of OER catalysis. According to the Tafel equation, Tafel slope was fitted from the LSV curves.[30,31] It can be seen from Fig. 3(b) that the Tafel slope of V–O_v–Co_3O_4 is 74.5 mV·dec^{-1}, which is smaller than that of Co_3O_4 (172 mV·dec^{-1}) and V–Co_3O_4 (152.9 mV·dec^{-1}), suggesting the rapid reaction kinetics of V–O_v–Co_3O_4. As displayed in Fig. 3(c), the overpotential and Tafel of among all as-prepared samples are put together to emphasize the improve of the OER activity of V–O_v–Co_3O_4. Furthermore, electrochemical impedance spectroscopy (EIS) test, a cogent method to analyses the electrode kinetics in electrocatalytic process, performed from high frequencies 100 kHz to low frequencies 0.1 Hz in 1.0-M KOH. The Nyquist diagram of V–O_v–Co_3O_4, V–Co_3O_4, and Co_3O_4 were compared under same potential in Fig. 3(d). Apparently, the semicircle of

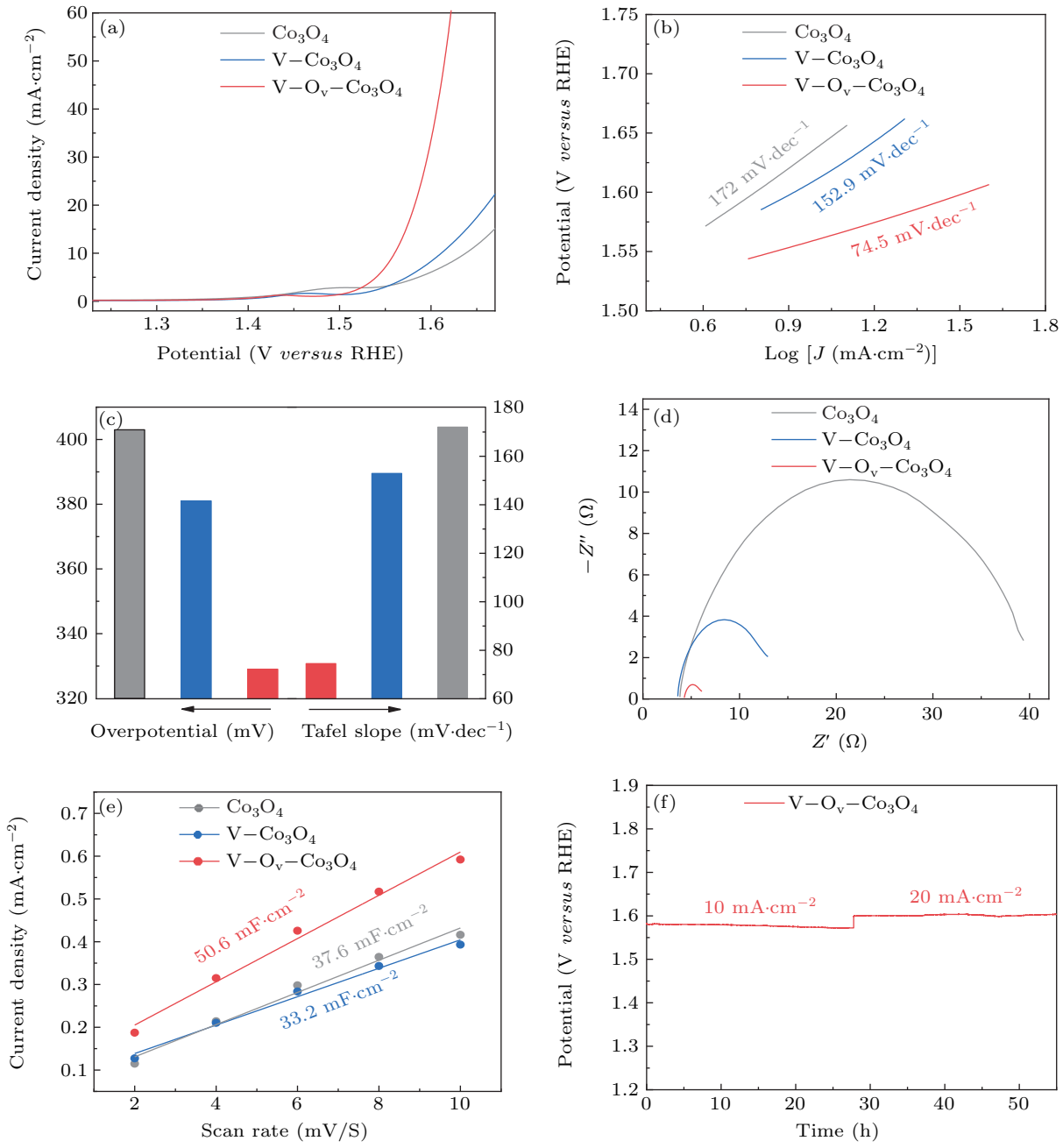


Fig. 3. Electrochemical catalytic measurement: (a) LSV curves of Co_3O_4, V–Co_3O_4, and V–O_v–Co_3O_4; (b) corresponding Tafel slopes of Co_3O_4, V–Co_3O_4, and V–O_v–Co_3O_4; (c) overpotential and Tafel slope of Co_3O_4, V–Co_3O_4, and V–O_v–Co_3O_4; (d) Nyquist plots of Co_3O_4, V–Co_3O_4, and V–O_v–Co_3O_4; (e) ECSAs of Co_3O_4, V–Co_3O_4, and V–O_v–Co_3O_4; (f) chronopotentiometric curves at 10 mA·cm^{-2} and 20 mA·cm^{-2}, respectively.

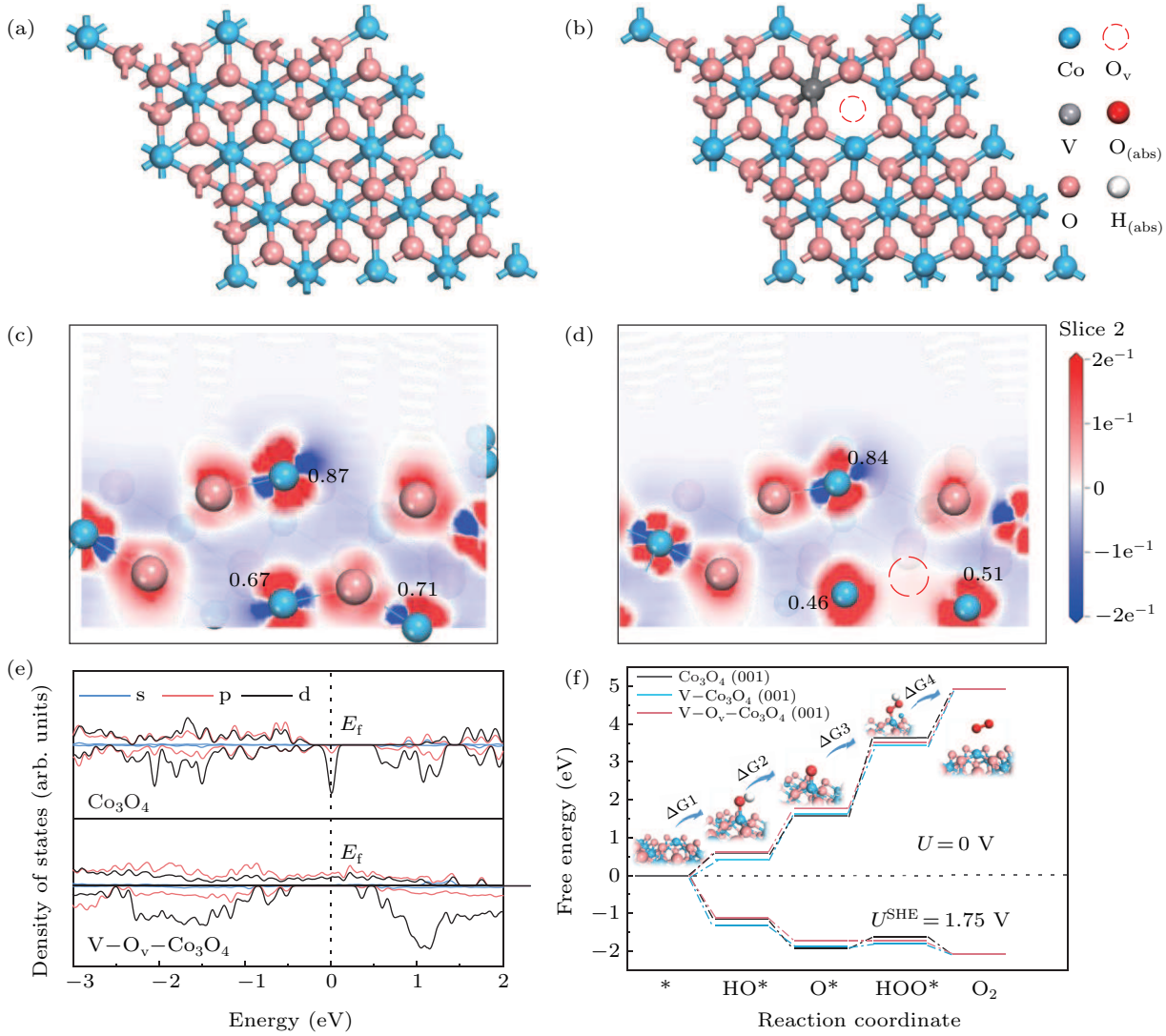


Fig. 4. DFT calculations of Co_3O_4 and V-implanted Co_3O_4. (a) The top view structures of Co_3O_4 (001) plane and $V–O_v–Co_3O_4$ (001). Slices of side view electron density differences of Co_3O_4 (c) and $V–O_v–Co_3O_4$ (d). (e) PDOS plots for Co_3O_4 and $V–O_v–Co_3O_4$. (f) The calculated OER Gibbs free energy diagrams.

$V–O_v–Co_3O_4$ at the high-frequency range in Nyquist diagram, is much smaller compared with Co_3O_4 and $V–Co_3O_4$, which indicated a smaller charge transfer resistance (R_{ct}). As show in Fig. S8, the charge-transfer resistance values of $V–O_v–Co_3O_4$ is 2.2 Ω, which is far less than of $V–Co_3O_4$ (10.3 Ω) and Co_3O_4 (34.9 Ω). The smaller R_{ct} suggest that high intrinsic activity performance can be ascribed to the great improvement interfacial electron-transfer kinetics and improved electrical conductivity. It is well known that the activity of a catalyst depends on the number of active centers and the inherent activity of each active centers. It is a widely recognized method to compare the electrochemical active surface area (ECSA) by measuring the electrochemical double-layer capacitance (C_{dl}). The C_{dl} was obtained by measuring the $C–V$ curve at different scan rates (Fig. S5).[32] As shown in Fig. 3(e), the C_{dl} of $V–O_v–Co_3O_4$ is 50.6 mF·cm^{-2}, higher than that of the Co_3O_4 (37.6 mF·cm^{-2}). The C_{dl} of $V–Co_3O_4$ (33.2 mF·cm^{-2}) is similar than that of Co_3O_4, which due to the reduction in the number of active sites caused by defect repair during thermal annealing. This confirms that high-energy V-ion implantation produced and exposed more active sites. Moreover, the long-term stability is crucial factors of the OER catalyst. The stability measure of $V–O_v–Co_3O_4$ was tested by chronopotentiometric curves at 10 mA·cm^{-2} and 20 mA·cm^{-2} for continuous 27 h, respectively. Indicating a good durability without appreciable increase in potential (Fig. 3(f)). The OER activity of three samples indicate that V-ion implantation is an efficient and stable method to generate oxygen vacancies and dope V element in Co_3O_4 for improving electrochemical activity. From the point of view of the reaction process, it is essential to in-depth investigate the mechanism of oxygen vacancy and vanadium doping to enhance the activity of OER.

Through density functional theory (DFT) calculations, the effects of oxygen vacancies and V doping on the electronic and catalytic properties of Co_3O_4 at the atomic level were studied. As shown in Fig. 4(a), the Co_3O_4 (001) crystal plane was first constructed, V-doped Co_3O_4 ($V–Co_3O_4$, Fig. S5) and coexistence models of V and oxygen vacancies

($V–O_v–Co_3O_4$, Fig. 4(b)) were also constructed by V atom replacing and oxygen atom removing. As shown in Figs. 4(c) and 4(d), due to the V doping and the oxygen vacancies caused by V ion implantation, the excess electrons generated by the oxygen vacancies are completely redistributed to the surrounding Co atoms, resulting in a decrease in the chemical state of the Co element compared with the original Co_3O_4, which is consistent with the result of XPS test. It can be clearly seen that the Millikan charge value of the exposed Co atom at the surface decreased from 0.87 to 0.84, which means that the charge density of the Co atom has increased. Therefore, its electronic structure can be effectively modulated to affect its catalytic activity. In addition, we found that the introduction of oxygen vacancies and V impurities can effectively adjust its band structure (Fig. 4(e)). It can be seen that oxygen vacancies and V doping can introduce a large number of impurity states in the Co_3O_4 band gap, thereby effectively enhancing the conductivity of the sample and accelerating its charge transfer process. The results are consistent with the EIS test data.

In order to further reveal the enhancement essence of V-ion implantation on catalytic activity from the perspective of the reaction mechanism, we calculated the energy profile of OER reaction pathway as shown in Fig 4(f).[33–35] It can be found that the limiting energy barrier of OER reaction pathway is from O^* to HOO^* step for Co_3O_4 (001) plane (Fig. S7). There is a 2.05 eV energy barrier for OER reaction. Interestingly, as a result of V-ions implantation, the adsorption capacity of the Co_3O_4 surface for OOH groups increases as the charge density of Co atoms increases, so the OER reaction barrier is effectively reduced. The OER reaction barriers of $V–Co_3O_4$ and $V–O_v–Co_3O_4$ are reduced from 2.05 eV to 1.82 eV and 1.75 eV, respectively. This calculation result is fully coupled with the LSV test, which provides an in-depth analysis of the enhancement mechanism of ion implantation.

3. Conclusion

In summary, we have confirmed that introducing V dopant and oxygen vacancy can significantly improve the OER activity of Co_3O_4. XPS, EDS, and DFT consistently proved that V-doping and oxygen vacancy produced by V-ion implantation effectively regulated the electronic density of Co_3O_4, which increased the electrical conductivity of Co_3O_4 and obviously decreased the energy barrier from O^* to HOO^*. The reducing of the reaction barrier is attributed to the improved HOO^* absorption. The optimized $V–O_v–Co_3O_4$ shows a lower overpotential of 329 mV, compared with Co_3O_4 (403 mV) and $V–Co_3O_4$ (381 mV). Also, $V–O_v–Co_3O_4$ has a low Tafel slope of 74.5 $mV·dec^{-1}$. Therefore, ion implantation can be used precise approach to manipulating electronic properties of metal oxide based OER catalysts.

References

[1] Zou X X and Zhang Y 2015 *Chem. Soc. Rev.* **44** 5148
[2] Hu C L, Zhang L and Gong J L 2019 *Energy Environ. Sci.* **12** 2620
[3] Wang M Y, Wang Z, Gong X Z and Guo Z C 2014 *Renewable Sustainable Energy Rev.* **29** 573
[4] Luo J S, Im J H, Mayer M T, Schreier M, Nazeeruddin M K, Park N G, Tilley D, Fan H J and Grätze M 2014 *Science* **345** 1593
[5] Risch M, Ringleb F, Kohlhoff M, Bogdanoff P, Chernev P, Zaharievaa I and Dau H 2015 *Energy Environ. Sci.* **8** 661
[6] McKone J R, Marinescu S C, Brunschwig B S, Winkler J R and Gray H B 2014 *Chem. Sci.* **5** 865
[7] Xu M Z, Li Q, Lv Y Y, Yuan Z M, Guo Y X, Jiang H J, Gao J W, Di J, Song P, Kang L X, Zheng L, Zhang Z Y, Zhao W, Wang X W and Liu Z 2020 *Tungsten* **2** 203
[8] You B and Sun Y J 2018 *Acc. Chem. Res.* **51** 1571
[9] She Z W, Kibsgaard J, Dickens C F, Chorkendorff I, Nørskov J K and Jaramillo T F 2017 *Science* **355** eaad4998
[10] Wu Y C, Ringe S, Wu C L, Chen W, Yang A, Chen H, Tang M, Zhou G, Hwang H Y, Chan K and Yi Cui 2019 *Nano Lett.* **19** 7293
[11] Pi Y C, Zhang N, Guo S J, Guo J and Huang X Q 2016 *Nano Lett.* **16** 4424
[12] Wang Y C, Zhou T, Jiang K, Da P M, Peng Z, Tang J, Kong B, Cai W B, Yang Z Q and Zheng G F 2014 *Adv. Energy Mater.* **4** 1400696
[13] Zhang K, Zhang G, Qu J H and Liu H J 2018 *Small* **14** 1802760
[14] Wang J Y, Shen Y L, Wei G J, Xi W, Ma X M, Zhang W Q, Zhu P P and An C H 2020 *Sci. China Mater.* **63** 91
[15] He D, Song X Y, Li W Q, Tang C Y, Liu J C, Ke Z J, Jiang C Z and Xiao X H 2020 *Angew. Chem. Int. Ed.* **59** 6929
[16] Ma T Y, Dai S, Jaroniec M and Qiao S Z 2014 *J. Am. Chem. Soc.* **136** 13925
[17] Firas F, Stumm C, Bertram M *et al.* 2018 *Nat. Mater.* **17** 592
[18] Zhang X Y, Li J, Yang Y, Zhang S, Zhu H H, Zhu X Q, Xing H H, Zhang Y L, Huang B L, Guo S J and Wang E K 2018 *Adv. Mater.* **30** 1803551
[19] Wang Z C, Xu W J, Chen X K, Peng Y H, Song Y Y, Lv C X, Liu H L, Sun J W, Yuan D, Li X Y, Guo X G, Yang D J and Zhang L X 2019 *Adv. Funct. Mater.* **29** 1902875
[20] Yuan H F, Wang S M, Mab Z Z, Kunduc M, Tanga B, Lib J P, Wang X G 2021 *Chem. Eng. J.* **404** 126474
[21] Zhu K Y, Shi F, Zhu X F and Yang W S 2020 *Nano Energy* **73** 104761
[22] Xiao Z H, Huang Y C, Dong C L, Xie C, Liu Z J, Du S Q, Chen W, Yan D F, Tao L, Shu Z W, Zhang G H, Duan H G, Wang S Y, Zou Y Q, Chen R and Wang S Y 2020 *J. Am. Chem. Soc.* **142** 12087
[23] Ahmed B, Aya E A and Ahmed A W 2021 *ChemSusChem* **14** 10
[24] Anindita, Singh A and Singh R N 2010 *Int. J. Hydrogen Energy* **35** 3243
[25] Jiang J, Sun F F, Zhou S, Hu W, Zhang H, Dong J C, Jiang Z, Zhao J J, Li J F, Yan W S and Wang M 2018 *Nat. Commun.* **9** 2885
[26] Liu J Z, Ji Y F, Nai J W, Niu X G, Luo Y, Guo L and Yang S H 2018 *Energy Environ. Sci.* **11** 1736
[27] Xu L, Jiang Q Q, Xiao Z H, Li X G, Huo J, Wang S Y and Dai L M 2016 *Angew. Chem. Int. Ed.* **128** 5363
[28] Wang Y C, Zhou T, Jiang K, Da P M, Peng Z, Tang J, Kong B, Cai W B, Yang Z Q and Zheng G F 2014 *Adv. Energy Mater.* **4** 1400696
[29] Song X Y, He D, Li W Q, Ke Z J, Liu J C, Tang C Y, Cheng L, Jiang C Z, Wang Z Y and Xiao X H 2019 *Angew. Chem. Int. Ed.* **58** 16660
[30] Shi H H, Liang H F, Ming F W and Wang Z C 2017 *Angew. Chem. Int. Ed.* **56** 573
[31] Shi H H, Liang H F, Ming F W and Wang Z C 2017 *Angew. Chem.* **129** 588
[32] McCrory C C L, Jung S, Peters J C and Jaramillo T F 2013 *J. Am. Chem. Soc.* **135** 16977
[33] Pham H H, Cheng M J, Frei H and Wang L W 2016 *ACS Catal.* **6** 5610
[34] Man I C, Su H Y, Calle-Vallejo F, Hansen H A, Martínez J I, Inoglu N G, Kitchin J, Jaramillo T F, Nørskov J K and Rossmeisl J 2011 *ChemCatChem* **3** 1159
[35] Aftab U, Tahira A, Mazzaro R, Morandi V, Abro M I, Baloch M M, Syed J A, Nafady A and Ibupoto Z H 2020 *Tungsten* **2** 403